

# Battery Abuse Case Study Analysis Using LS-DYNA<sup>®</sup>

James Marcicki<sup>1</sup>, Alexander Bartlett<sup>1</sup>, Xiao Guang Yang<sup>1</sup>, Valentina Mejia<sup>1</sup>,  
Min Zhu<sup>1</sup>, Yijung Chen<sup>1</sup>, Pierre L'Eplattenier<sup>2</sup>, Iñaki Çaldichoury<sup>2</sup>

<sup>1</sup>Ford Research and Innovation Center, Dearborn, MI, USA

<sup>2</sup>LSTC, Livermore, CA, USA

## Abstract

*Battery abuse research and modeling, Spatially-resolved battery modeling, Electro-thermal battery modeling.*

*As Lithium-ion batteries see increasing use in a variety of applications, anticipation of the response to abuse conditions becomes an important factor in designing optimized systems. Abuse scenarios with potential relevance to the automotive industry include crash-induced crush leading to an internal short circuit, external short circuit, or thermal ramp, and overcharge conditions. Simulating each of these abuse scenarios requires sophisticated modeling tools that span multiple physical and electrochemical phenomena, as well as handle complex geometries that accurately represent battery cells, modules, and packs.*

*The three-dimensional, transient analysis capabilities of LS-DYNA can be leveraged to simulate the battery response with a high degree of spatial resolution, which is widely considered a prerequisite for predicting the highly localized phenomena involved in the onset of thermal runaway. The electrical, electrochemical and thermal response of the new LS-DYNA battery model can be coupled to the mechanical solver using a variety of approaches, ranging from one-way coupling based on a time-scale analysis to tight two-way coupling.*

*Several battery abuse case studies will be examined to verify the capability of the modeling tools. The impact of hardware size will be investigated, as the thermal behavior and corresponding severity of the abuse response changes depending on the number of cells and their configuration within a module. Experimental data will be used to estimate parameters, confirm the model capability, and identify areas of future work to improve the fidelity and ease of implementation of the simulation tool. Multiple hardware types will be compared to demonstrate the relationship between cell performance and module abuse response.*

## 1-Introduction

Delivering safe battery pack designs is a key requirement for the development of electrified vehicles. Testing at the component-level can provide useful insight into the abuse tolerance of Li-ion cell technologies, but computer aided engineering (CAE) tools can provide further insight into how components respond as part of a larger module or pack system. Therefore, battery CAE tool development has the potential to reduce costs associated with the process of designing and building prototypes followed by extensive testing by reducing the number of iterations required and accelerating the rate at which designs can be analyzed. As with most other automotive components, it is generally assumed three-dimensional, transient, finite element analysis is needed to support virtual verification of a battery pack design. National laboratories and academic research groups have developed insightful models [1,2] for various abuse scenarios, but there are limited commercially available options that support a large user base. Models have been proposed for strictly mechanical predictions [3, 4], but results from these models are difficult to integrate into predictions of whether thermal runaway occurs without explicitly simulating the subsequent thermal and electrical consequences of mechanical failure. Thermal

or coupled thermal and electrical models have also been pursued [5, 6], but commercially available tools that can span all sets of physics have the potential to advance battery CAE.

To support the goal of virtual verification of battery systems, Ford and LSTC are collaborating on the development of new keywords and solver enhancements for battery abuse response. The mathematical description, assumptions, implementation, and validation for nominal cycling cases is described in Ref [7]. In this paper, external and internal short circuit scenarios are analyzed using a three-dimensional, electrothermal model. Experimental data is used to estimate parameters and confirm the capability of the model to represent experimentally observed trends. Results are presented at the cell-level and module-level to demonstrate the relationship between cell performance and module abuse response, and the importance of accurately representing the mechanical configuration of cells and their connections to electrical bus connections. Areas of future work to improve the model fidelity are also discussed.

## 2-Experimental Design

### 2-1 Internal Short Circuit

An internal short circuit occurs when the battery separator fails to prevent mechanical contact between the positive and negative battery electrodes. This is a possible failure mode when extreme mechanical loads are applied to battery hardware. In order to study the onset of internal short circuits, a set of impact experiments were conducted by the Ford Energy Storage Research team in collaboration with NREL. In these experiments, a rod of 20kg mass was dropped from 2m high (maximum 6.3 m/s impact velocity) onto a single Type A cell. The voltage of the cell, temperatures at various locations, and strain were recorded at 100 Hz, while the impact force was recorded at 10 kHz. Pictures of the impact event obtained using a high-speed camera are shown in **Fig. 1**. Despite the impact event creating a short circuit, the cell did not undergo thermal runaway but rather discharged at a moderate rate leading to a benign temperature rise above ambient conditions.

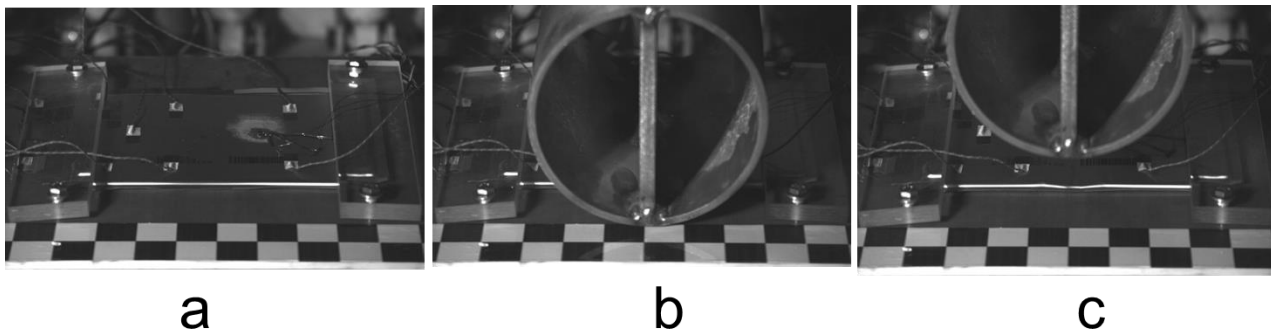


Figure 1: Experimental setup for the rod impact experiment showing the cell with the different diagnostics before impact (a), the plate and rod at impact (b), and the rod and plate just after the first rebound (c), before settling.

### 2-2 External Short Circuit

An external short circuit is classified as a current pathway outside of a battery cell that directly connects the positive and negative terminals. At high resistances an external short scenario produces a benign thermal response, but if a low-resistance pathway is created the resulting

currents can be high and greater possibility for heating is present. From 2011 to 2014, Ford Energy Storage Research conducted a project focused on developing Li-ion battery safety test procedures. As part of that effort, external short circuit tests were conducted for a variety of hardware types, including the 1S4P module presented in this paper. The current that flows after creating the external short connection, and the resulting voltage and temperature of the module are recorded at 10 Hz. Thermocouples are located on the positive and negative bus bars as well as the center of the cell surface.

### 3-Electrothermal Model Development

#### 3-1 Distributed Randle Model

The \*EM\_CIRCUIT\_RANDLE keyword has been developed to model the electrochemical response of Li-ion battery active materials. When this keyword is activated, opposing segment sets on conductive materials are recognized to contain a battery unit cell consisting of negative electrode active material, a porous separator, and positive electrode active material. The electronic current delivered by each unit cell is supplied to the standard EM Resistive Solver, which computes the solution to the Laplacian equation for the scalar potential at the conductor nodes. The electrochemical consequences of the ionic current that passes between opposing unit cell electrodes are modeled using the first order Randle circuit analogy. Further details regarding the assumptions, implementation, and validation of the \*EM\_CIRCUIT\_RANDLE keyword and coupling to the Thermal Solver are discussed in Ref [7].

#### 3-2 Internal Short Circuit

The internal short circuit analysis of this paper consists of a coupled EM and thermal simulation, where pure resistive elements replace the Randle circuit in regions with an assumed short circuit. The cell mechanical response is not included in this preliminary simulation for several reasons. First, the mechanical simulation of such a composite material with extremely small layer thicknesses and vastly different stiffnesses is very challenging. Additionally, in this particular example, the impact event occurs within a few hundred milliseconds. Therefore, the time scale of the thermal response is orders of magnitude slower. Finally, removal of the mechanics allows testing of the voltage and thermal models by deriving an apparent short circuit resistance from the experimental data, without introducing additional mechanical uncertainties.

Additional support for the assumption that the EM and thermal processes occur over a much longer time scale is now discussed. For the particular relationship between open-circuit voltage (OCV) and state-of-charge (SOC), the cell behaves like a capacitor with  $C = 1.2 \times 10^5 F$ , and the internal resistance is approximately  $r_0 = 1.4 \times 10^{-3} \Omega$ . This implies that if an internal short occurs, with a resistance  $r_s$ , the discharge of C in  $r_0 + r_s$ , and Joule heating associated with  $r_s$  will happen in a characteristic time  $t_d = (r_0 + r_s)C \geq r_0 C = 183s$ . This is clearly much larger than the impact time which in this experiment occurs in less than 1s. To summarize the process, the impact occurs quickly, creates a short circuited area with an associated resistance, and the remaining functional areas of the cell discharge in that resistance, generating heat in the process.

Since the rod was 15cm diameter, we decided to apply a shorted region between 3 and 4 cm wide, going across the full thickness of the cell. **Fig. 2** shows the mesh of the cell along with the shorted area, i.e. the nodes where the Randle circuits were switched to a resistance. These nodes represent  $8 \times 30 = 240$  shorted circuits out of a total of 1200 Randle circuits per unit cell.

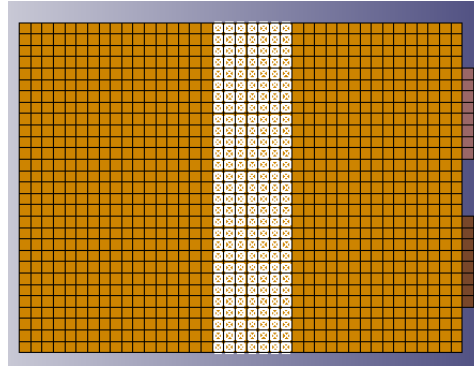


Figure 2: Mesh of the cell along with the nodes with internal shorts (connected to elements with white x indications)

To estimate the resistance of the internal short circuit, the following method is applied. **Fig. 3** shows a lumped first order Randle circuit discharging in an internal resistance. If we sum up the tensions we get:

$$u - R_S i - v_c - R_0 i = 0 \tag{1}$$

With  $v_s = R_S i$

which also reads, after some rearrangements:

$$R_S = \frac{v_s}{u - v_s - v_c} R_0 \tag{2}$$

Since  $v_s(t)$  is experimentally measured, and the simulation gives us  $u$  and  $v_c$  at each time step, we can get an estimate for  $R_S(t)$  which we evenly split between the 7680 shorted circuits in the entire cell.

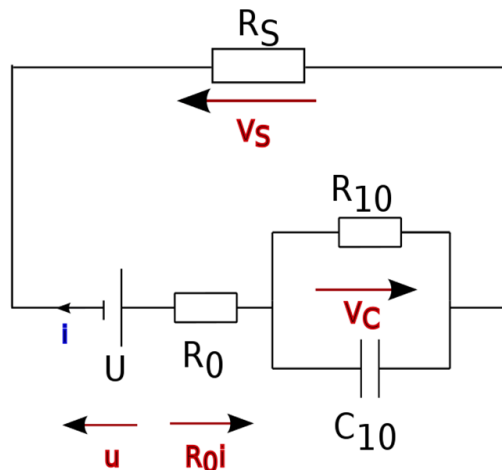


Figure 3: Lumped first order Randle circuit discharging in an internal resistance  $R_S$ .

### 3-3 External Short Circuit

The characteristics of the Type A cell mesh are described in Ref [7]. The module analyzed in this work consists of four cells connected electrically in parallel (1S4P), which leads to a total element count of approximately 650k. No other changes are made to the cell mesh resolution, though larger modules or packs may require a larger in-plane element size or reducing the number of explicitly modeled unit cells to avoid excessively large element counts.

Thermal connections between cells within the module, and between cell tabs and the bus bar, are implemented using \*CONTACT\_SURFACE\_TO\_SURFACE\_THERMAL. Isopotential surfaces are created on the edge of each tab and the lower bus bar surface by creating node sets at these locations and inputting them into \*EM\_ISOPOTENTIAL. Each cell positive and negative tab is then connected electrically to the corresponding bus bar using \*EM\_ISOPOTENTIAL\_CONNECT.

External short circuits are implemented by connecting the positive and negative bus bars with a time-varying resistance profile obtained from experiments, also controlled with \*EM\_ISOPOTENTIAL\_CONNECT. The resistance of these inert bus bars is computed using an equation of state (EOS) that depends linearly on temperature. These connections are summarized in **Fig. 4**.

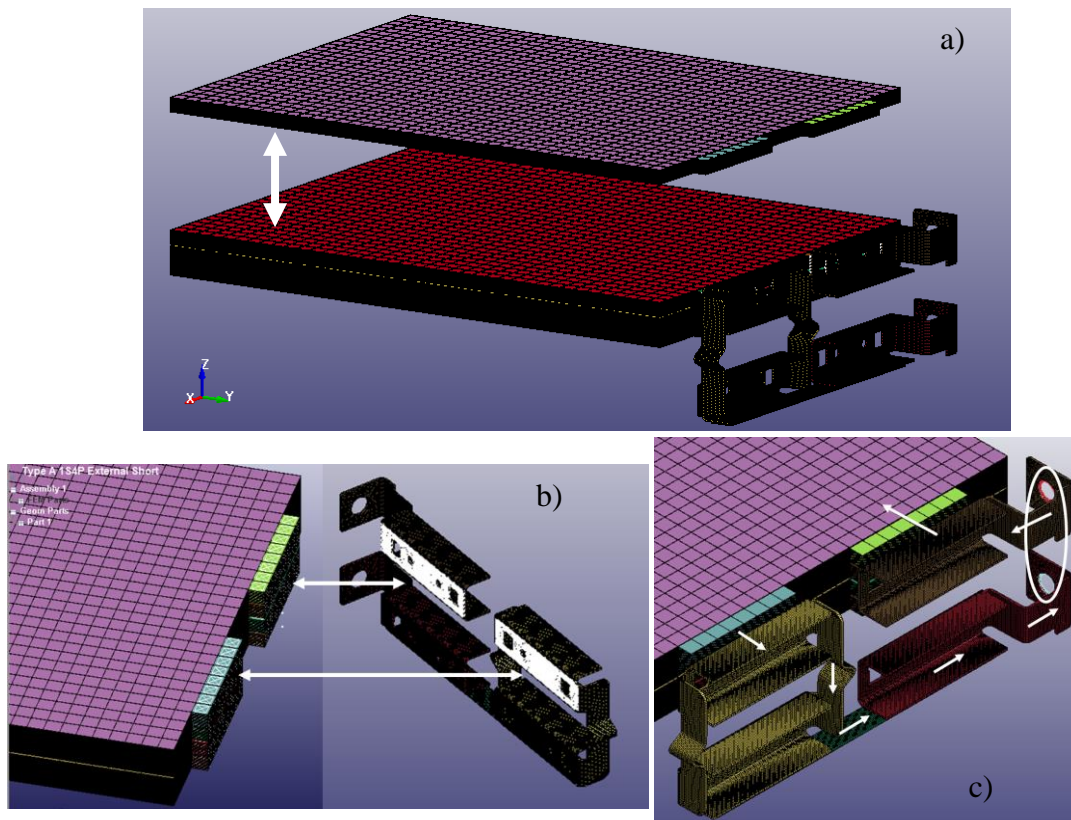


*Figure 4: Connections applied to cells to create a module configuration. a) Cell-to-cell heat transfer indicated by white arrow with spacing exaggerated for clarity. b) Cell-to-bus heat transfer and electrically conductive pathways. c) External attachment points indicated by highlighted node sets and white oval, and resulting conventional current pathway indicated by white arrows.*

## 4-Results and Discussion

### 4-1 Internal Short Circuit

**Fig. 5** shows the experimentally measured voltage versus time, which shows on the left the slow discharge of the cell in the internal short, taking about 1600s. In the zoomed picture on the right, we can clearly see the first impact of the rod near 7.8s, followed by a rebounding of the rod away from the cell surface, and the second impact near 8.2s. The right plot also demonstrates the difference between the cell voltage,  $v$ , and the initial OCV,  $u_0$ , which can be used to approximately compute the short circuit resistance at early time if we assume the OCV and  $v_c$  do not change instantaneously from their initial values. Mathematically we have:

$$R_S \approx \frac{v_s}{u_0 - v_s} R_0 \quad (3)$$

In practice, **Eq. 3** is used for the evaluation of  $R_S$ , with dynamic updates to the state variables as current is passed. **Fig. 6** shows the resistance vs time that was computed using **Eq. 3** and injected into the LS-DYNA simulation using a load curve, after evenly distributing the value across the shorted Randle nodes using area-based scaling. A log axis is used to plot the time series since the resistance varies by orders of magnitude in time, appearing to be proportional to the measured force between the cell and the impactor (not shown). Resistance values nearly as low as 10 mOhms are experienced during the initial impact, settling to approximately 100 mOhm over the course of a few seconds. This corresponds to the reaction force decreasing to merely support the resting weight of the impactor.

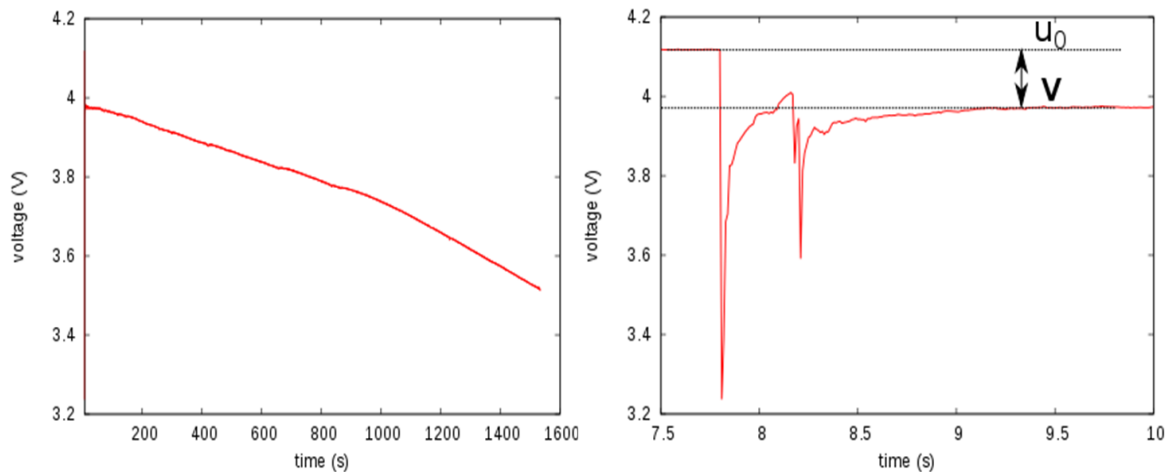


Figure 5: measured voltage versus time for the whole discharge (left) and around the impact (right).

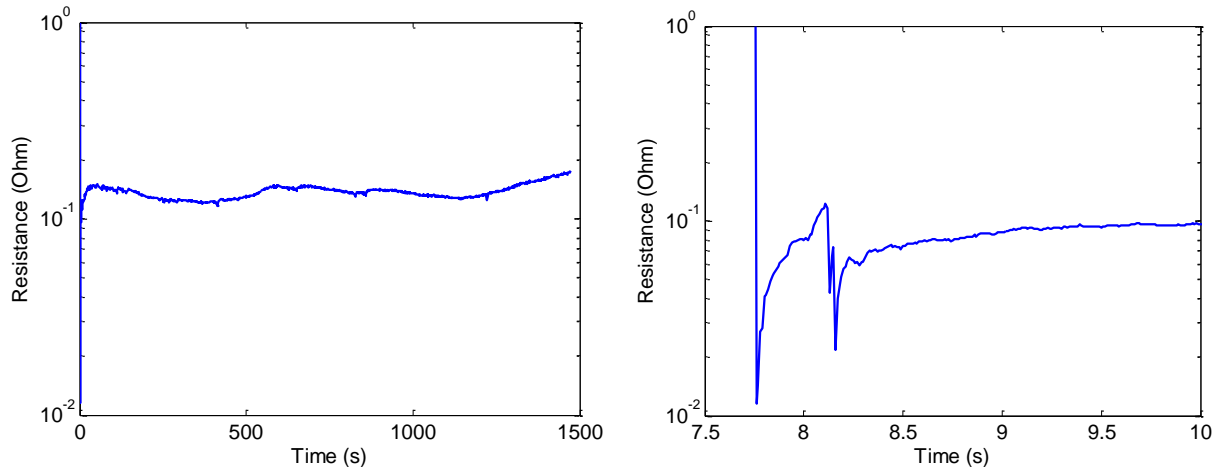


Figure 6: Computed short resistance versus time for the whole discharge (left) and around the impact (right).

**Fig. 7** shows the numerical and experimental voltage time series with good agreement throughout the discharge. The dynamic variations that happen in the first few seconds are captured well, and the long term discharge rate also agrees with the experiments as shown by the similar trends in voltage for hundreds of seconds following the impact. **Fig. 8** shows the scalar potential, current density and Randle current  $i$  after the short, which clearly demonstrates where the short circuit took place. In a normal discharge, current density vectors would be predominantly uniform and directed towards the external tab locations at the top of the cell. With the introduction of the internal short, the cell is bisected into two regions above and below the shorted area. Functioning areas of the cell closer to the shorted location supply more current than those positioned further away due to the coupling between the electrochemical response, the ohmic drop within the current collectors, and the persistent temperature gradient.

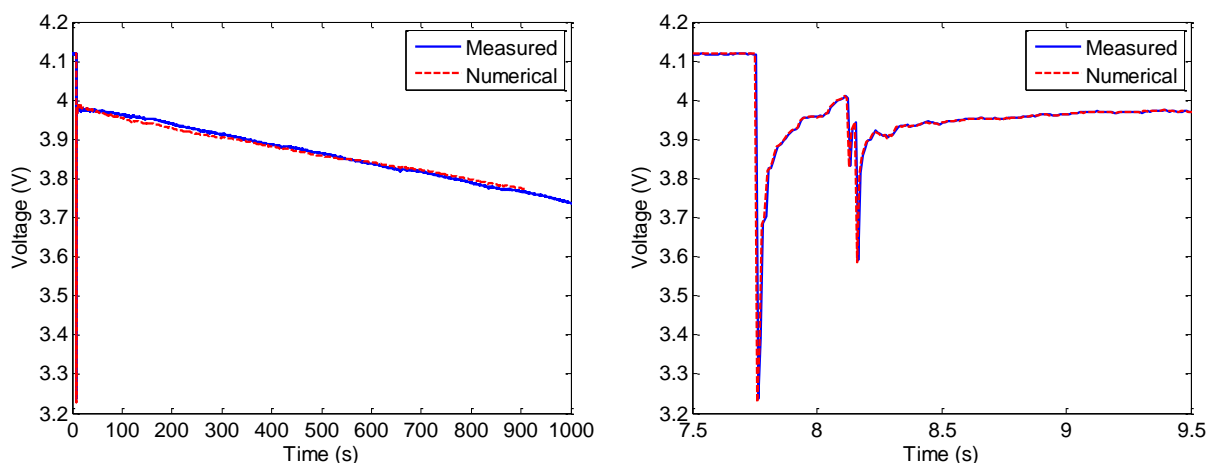


Figure 7: Measured and numerical voltage for the whole discharge (left) and zoomed at the impact (right).

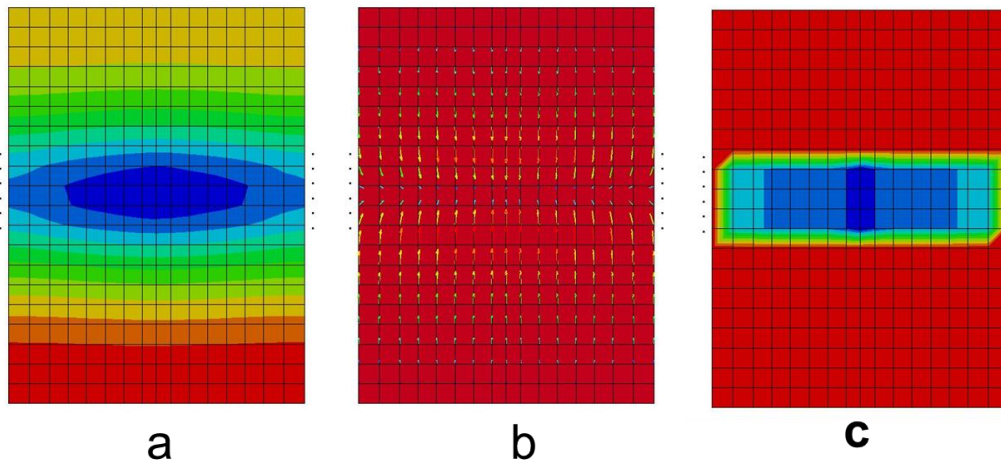


Figure 8: Scalar potential (a), current density (b) and Randle current  $i$  (c) after the impact and the onset of the short. Normal operation would feature a mostly uniform current density with some localization near the external tabs, for instance see Fig. 11 of Ref. [7].

The thermal aspect of this case study is complicated by the uncertainty surrounding the contact between the rod and the cell, as well as the heat transfer coefficients between the rod and the ambient air. Following the impact and a short rebounding period, the rod comes to rest on top of the cell and therefore offers a large heat sink during the subsequent discharge period. This thermal transfer is modeled using \*CONTACT\_SURFACE\_TO\_SURFACE\_THERMAL, but uncertainties remain surrounding the resting contact area between the cell and the rod, as well as the heat transfer conductance, leading to inaccuracies between the observed peak temperatures and the time scales required to reach the peak values. Additionally, no attempt was made to adjust the heat transfer coefficient between the cell and its ambient environment, or between the rod and the environment. The final temperature of the cell is approximately 80°C which represents a reasonable overestimation of the experimental values of over 50°C. Fig. 9 shows the temperature distribution of the cell and the rod as time elapses following the onset of the short circuit.

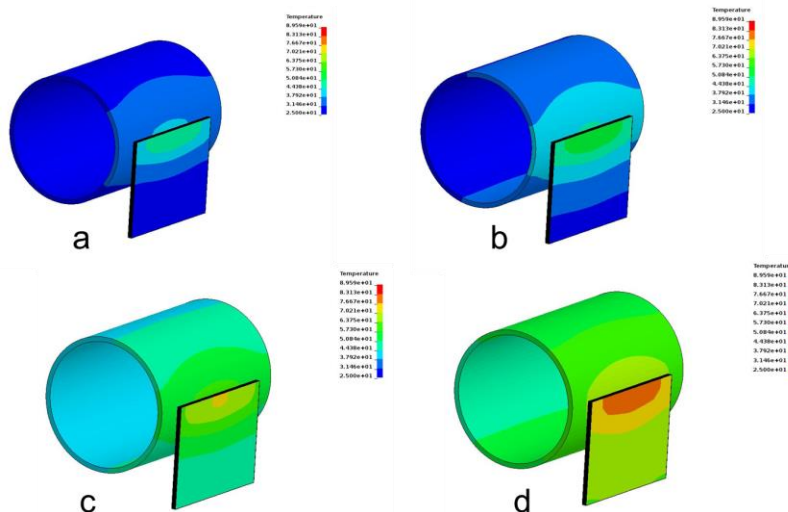


Figure 9: Cell (only 1/2 shown) and rod temperature fringes at  $t=100s$  (a),  $t=200s$  (b),  $t=500s$  (c) and  $t=1000s$  (c).

## 4-2 External Short

The external short simulation utilizes the experimentally measured resistance versus time curve from experiments as its input. Alternatively, a fixed resistance of arbitrary value can be applied to the terminals when performing parametric sweeps to determine the threshold resistance value below which the cell exhibits an unacceptable thermal response. **Fig. 10** shows the experimentally obtained resistance data, which is computed from the current and voltage measurements. This data is input into the LS-DYNA simulation as a load curve for \*EM\_ISOPOTENTIAL\_CONNECT type 2 to produce the voltage, current, and temperature results of **Fig. 11**.

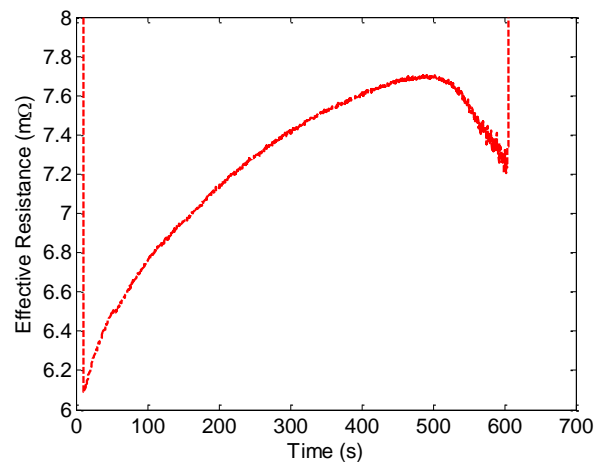


Figure 10: External short circuit resistance obtained from experiments. Data is stored as a load curve and used as the simulation input for \*EM\_ISOPOTENTIAL\_CONNECT type 2. Data outside the y-axis limits are resistances greater than 1 k $\Omega$  that impose an open-circuit condition.

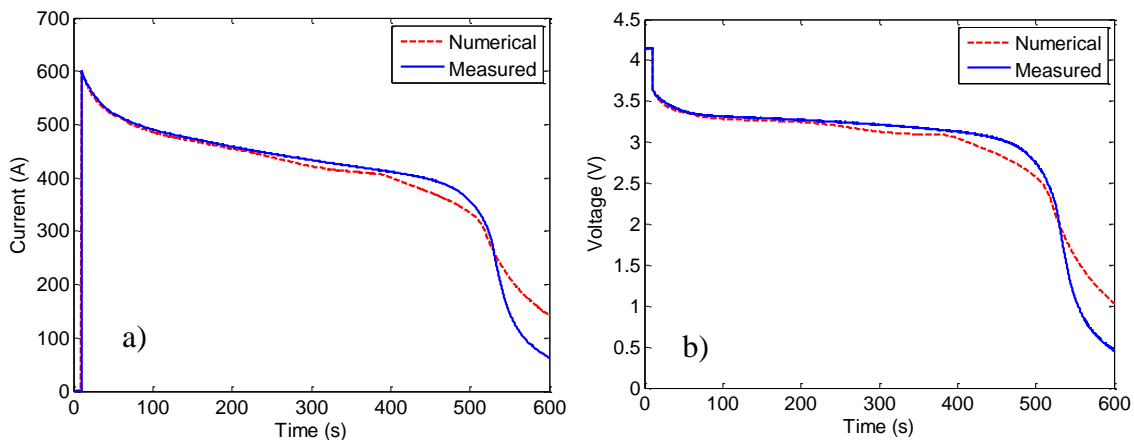


Figure 11: Comparison between model prediction and experimental measurements of a) current and b) voltage during the external short circuit. The cell is initially at rest and the short circuit is applied at 10s.

The model accurately predicts the peak current as well as the transient response after the short circuit is applied. Good agreement is also obtained for the voltage response, though to achieve this level of agreement, the capacity of the cell had to be increased by approximately ten percent compared with the value identified during the cell-level validation. It is believed this is related

to the assumption that the maximal capacity occurs for the 1C rate at 25°C, whereas in reality the cell may deliver a greater capacity at the higher temperatures experienced during the external short due to improved kinetics and reduced diffusion limitations. Still, both current and voltage results match with less than 7% error prior to 500s, when a majority of the cell energy is discharged.

The thermal response of the model is compared with the experiments in **Fig. 12**.

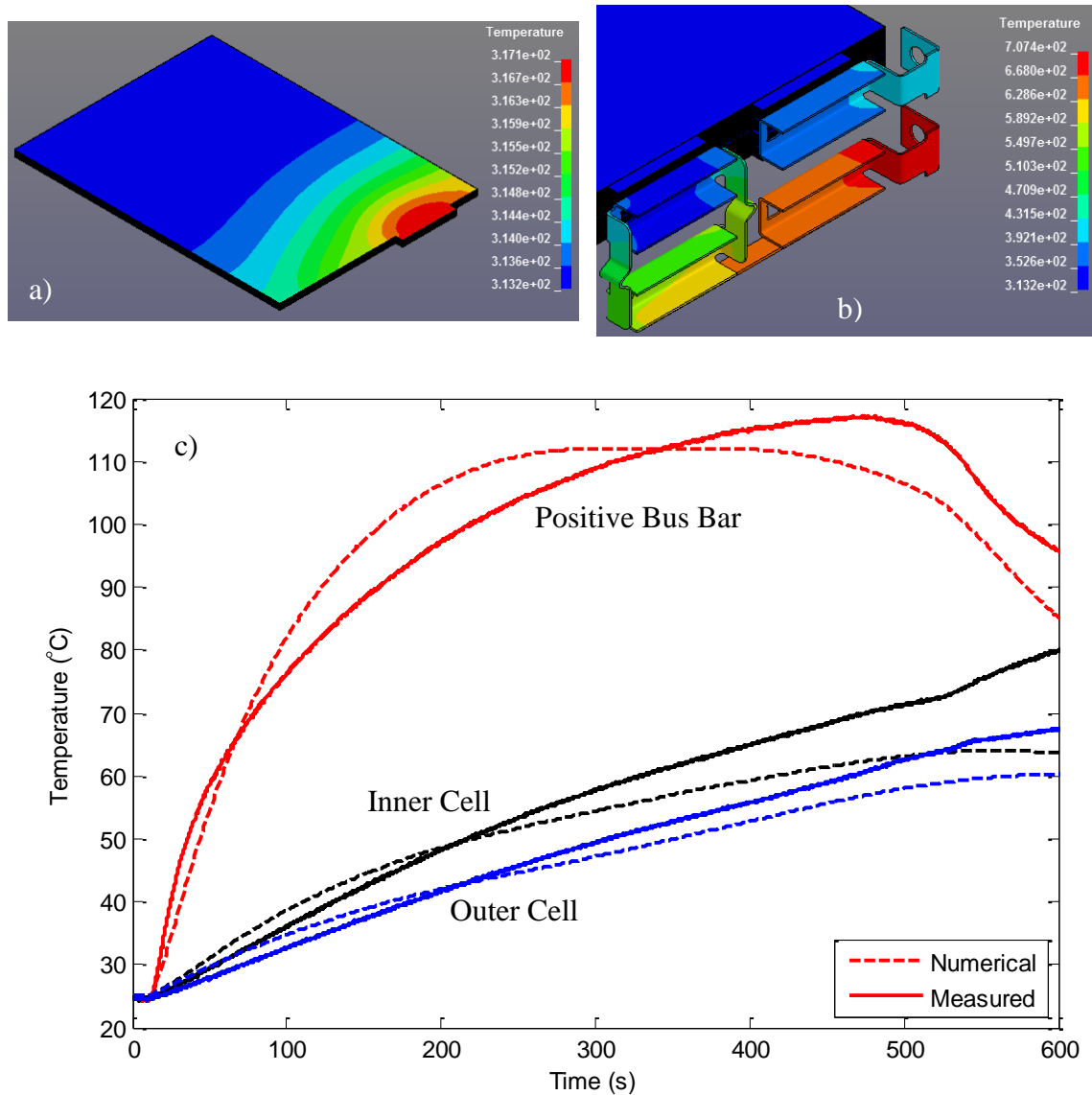


Figure 12: Thermal response of the external short circuit. a) Temperature fringe plot on the positive current collector surface for an outer cell. b) Temperature fringe plot on the bus bars. c) Comparison between experimental and simulated temperature time series data, where dashed lines indicate simulation results and solid lines are experimental measurements. Temperature fringe plots are shown at  $t = 267s$ , contain different scales due to the large temperature gradient between the bus bars and cells, and have units of Kelvin.

The selected thermal conductance value for the surface to surface contact between the bus bars and the cell tabs appears, as well as the meshed contact area, combine to reasonably capture the

temperature gradient that forms. Additionally, the initial temperature trends for times less than 200s agree well with the experiments. Eventually, the under prediction of the cell temperature for times greater than 200s causes a corresponding under prediction in the bus temperature. The model under predicts the temperature rise of the cells and bus bar, each by approximately ten to twenty degrees, which could be due to a number of factors. First, the model parameterization could have assigned too much voltage polarization to the SOC shift behavior. Although the shifted SOC is used to evaluate the resistance parameters which affect the irreversible heat generation, the polarization effect it causes does not directly contribute to heat generation. Reducing the magnitude of the SOC shift and increasing the cell internal resistance to maintain the same voltage polarization, or even slightly reduce the overall polarization to better match the current and voltage in the 400s to 500s range, would also improve the temperature predictions. Furthermore, it seems significant energy is stored in the negative, external bus bar. If more of this energy was transferred to the cells, it would also improve the thermal predictions for longer times. These factors will be investigated as part of future work involving the simulation of a broader range of Li-ion module types and sizes.

A parametric analysis can also be applied to the model to understand the relationship between the applied resistance and the propensity of the hardware to reach the onset temperatures of various processes, such as exothermic side reactions or separator melting. In particular, processes associated with the high temperature side reactions of lithiated graphite [8] are indicated on **Fig. 13**. Simulation results for three different external resistance values are shown, with labels that indicate the normalized resistance  $R_{ext}/R_{module}$ . Certain resistance ratio values, in this case less than 14, produce strong enough heating to push into regions where exothermic side reactions are possible.

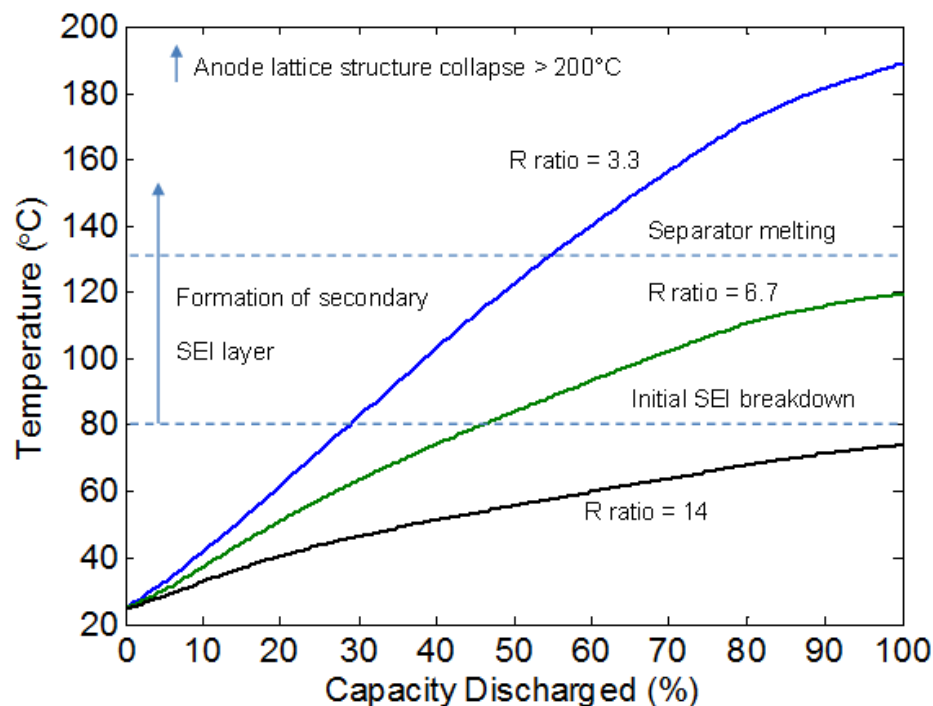


Figure 13: Thermal response of an inner cell versus capacity discharged during an external short scenario. The R ratio indicates the ratio of the externally applied resistance to that of the module.

The interpretation of the thermal response does not necessarily require constricting the final temperature below a constant value, but rather can be based upon material calorimetry data for various SOCs. It has been demonstrated that the impact of high temperatures is not uniform across the entire SOC range, and high temperatures at low SOC may not create a significant amount of heat generation as compared to high SOC [8].

## **5 Conclusion**

A circuit based battery model available in LS-DYNA has been used to analyze battery abuse scenarios. Data from internal and external short circuit experiments have been used to define simulation inputs and predict the resulting electrothermal response. The interaction between inert conductors and electrochemical cells required for module-level analysis has been modeled, indicating a non-negligible increase in the heat produced as compared to the cell-level. Although the process of identifying a consistent set of parameters that adequately represent the experimental data is still underway, the initial results demonstrate the model captures a number of key characteristics. Future work will focus on investigating a larger number of Li-ion module designs, including alternative chemistries, form factors, and sizes.

## **References**

- [1] C. Zhang, S. Santhanagopalan, M. Sprague, A. Pesaran, "Coupled mechanical-electrical-thermal modeling for short-circuit prediction in a lithium-ion cell under mechanical abuse", *J. Power Sources*, 290 (2015), 102 – 113.
- [2] W. Zhao, G. Luo, C.Y. Wang, "Modeling Nail Penetration Process in Large-Format Li-Ion Cells", *J. Electrochem. Soc.*, 162 (1), A207 – A217 (2015).
- [3] E. Sahraei, R. Hill, T. Wierzbicki, "Calibration and Finite Element Simulation of Pouch Lithium-Ion Batteries for Mechanical Integrity", *J. Power Sources*, 201, 307 – 321, (2012).
- [4] W. Lai, M. Ali, J. Pan, "Mechanical Behavior of Representative Volume Elements of Lithium-Ion Battery Modules Under Various Loading Conditions", *J. Power Sources*, 248, 789 – 808, (2014).
- [5] C. Lopez, J. Jeevarajan, and P. Mukherjee, "Characterization of Lithium-Ion Battery Thermal Abuse Behavior Using Experimental and Computational Analysis", *J. Electrochem. Soc.*, 162 (1), A2163 – A2173 (2015).
- [6] G. Guo, B. Long, B. Cheng, S. Zhou, P. Xu, and B. Cao, "Three-Dimensional Thermal Finite Element Modeling of Lithium-Ion Battery in Thermal Abuse Application", *J. Power Sources*, 195 (8), 2393 – 2398, (2010).
- [7] P. L'Eplattenier, I. Çaldichoury, J. Marcicki, A. Bartlett, X.G. Yang, V. Mejia, M. Zhu, Y. Chen, "A Distributed Randle Circuit Model for Battery Abuse Simulations Using LS-DYNA," presented at the 14th International LS-DYNA Conference, 2016.

[8] H. Yang, H. Bang, K. Amine, J. Prakash, “Investigations of the Exothermic Reactions of Natural Graphite Anode for Li-Ion Batteries during Thermal Runaway”, J. Electrochem. Soc., 152 (1), A73 – A79 (2005).

### **Acknowledgments**

For the experimental testing of internal short circuits, the Ford authors acknowledge the support of the Vehicle Technologies Office, Office of Energy Efficiency and Renewable Energy, U.S. Department of Energy under a subcontract from the National Renewable Energy Laboratory with DOE Agreement # 27627. For the experimental testing of external short circuits, the Ford authors acknowledge the support of the National Highway Safety Administration (NHTSA). The Ford authors also acknowledge that this work was supported by the Vehicle Technologies Office, Office of Energy Efficiency and Renewable Energy, U.S. Department of Energy under DOE Agreement DE-EE0007288.